Nuclear Science and Techniques (2025) 36:240
https://doi.org/10.1007/s41365-025-01829-7

A substitution measurement for cross section of ^{65}Cu(γ, n)^{64}Cu reaction using ^{nat}Cu and ^{63}Cu targets by quasi-monoenergetic γ beams at SLEGS

Pu Jiao[1,2] · **Zi-Rui Hao**[2] · **Zhi-Cai Li**[2,3] · **Qian-Kun Sun**[4,5] · **Long-Xiang Liu**[2] · **Hang-Hua Xu**[2] · **Yue Zhang**[2] · **Meng-Die Zhou**[1,2] · **Wen Luo**[3] · **Yu-Xuan Yang**[4,6] · **Sheng Jin**[4,5] · **Kai-Jie Chen**[4,7] · **Shan Ye**[2,8] · **Zhen-Wei Wang**[4,5] · **Yu-Ting Wang**[1] · **Hui-Ling Wei**[1] · **Yao Fu**[4,5] · **Kun Yu**[9] · **Hong-Wei Wang**[2,4,5] · **Gong-Tao Fan**[2,4,5] · **Chun-Wang Ma**[1,10]

Received: 15 April 2025 / Revised: 14 August 2025 / Accepted: 18 August 2025 / Published online: 17 October 2025

Abstract

To overcome the difficulty and high cost of some specific isotopic targets, a substitution method was proposed to measure the cross section of the (γ, n) reactions. Considering that the natural copper element (^{nat}Cu) only has ^{63}Cu and ^{65}Cu isotopes, the ^{65}Cu(γ, n)^{64}Cu reaction was taken as an example to test the substitution method. Using quasi-monoenergetic γ beams provided by the Shanghai Laser Electron Gamma Source (SLEGS) of the Shanghai Synchrotron Radiation Facility (SSRF), ^{nat}Cu(γ, n) was measured from $E_\gamma = 11.09$ MeV to 17.87 MeV. Furthermore, based on the ^{63}Cu(γ, n) reaction measured using the same experimental setup at SLEGS, ^{65}Cu(γ, n)^{64}Cu was extracted using the substitution method. The abundance variation of natural copper, showing a significant influence on the cross section, was also investigated. The results were compared to the existing experimental data measured by bremsstrahlung and positron annihilation in-flight sources, and the TALYS 2.0 predictions. The γ strength function (γSF) of ^{65}Cu was obtained from the ^{65}Cu(γ, n) data, and the reaction cross section of ^{64}Cu(n, γ) was further calculated.

Keywords Photoneutron cross section · Flat-efficiency detector · Laser Compton scattering · γ rays · SLEGS · Substitution measurement · Copper isotopes

---

Pu Jiao and Zi-Rui Hao contributed equally to this work.

This work was supported by the National key R&D program (Nos. 2022YFA1602404 and 2023YFA1606901), the National Natural Science Foundation of China (Nos. 12375123 and 12388102), and the Natural Science Foundation of Henan Province (No. 242300422048).

✉ Gong-Tao Fan
fangt@sari.ac.cn

✉ Chun-Wang Ma
machunwang@126.com

[1] School of Physics, Centre for Theoretical Physics, Henan Normal University, Xinxiang 453007, China

[2] Shanghai Advanced Research Institute, Chinese Academy of Sciences, Shanghai 201210, China

[3] School of Nuclear Science and Technology, University of South China, Hengyang 421001, China

[4] Shanghai Institute of Applied Physics, Chinese Academy of Sciences, Shanghai 201800, China

[5] University of Chinese Academy of Sciences, Beijing 101408, China

[6] School of Physics, Zhengzhou University, Zhengzhou 450001, China

[7] ShanghaiTech University, Shanghai 201210, China

[8] China Institute of Atomic Energy, Beijing 102413, China

[9] Henan Key Laboratory of Infrared Material & Spectrum Measures and Applications, Henan Normal University, Xinxiang 453007, China

[10] Institute of Nuclear Science and Technology, Henan Academy of Sciences, Zhengzhou 450046, China

1 Introduction

The ^{65}Cu(γ, n)^{64}Cu reaction has important medical and scientific applications [1, 2]. ^{64}Cu is a short-life β^+ emitter ($T_{1/2}$ = 12.7 h; β^+ with a mean energy of 278 keV, a branching ratio of 61.5%, and β^- with a mean energy of 191 keV and a branching ratio of 38.5%), which is widely used in nuclear medical imaging techniques such as positron emission tomography (PET) [3, 4] and single-photon emission computed tomography (SPECT) [5] and plays an important role in clinical diagnosis. For example, ^{64}Cu-labeled peptides such as ^{64}Cu-DOTATATE [1, 6] are used in the diagnosis of neuroendocrine tumors [7], ^{64}Cu-labeled oxygen depletion probes, such as ^{64}Cu-ATSM [8], are used to detect oxygen depletion regions in tumors, and ^{64}Cu-labeled prostate-specific membrane antigen (PSMA) [9] ligands are used in PET imaging of prostate cancer to precisely localize tumor cells. In addition, ^{64}Cu can be used in radionuclide therapy to destroy tumor cells through the decay properties of β^+ and β^- [10]. The ^{65}Cu(γ, n)^{64}Cu reaction is also of great importance in scientific research. For example, in nuclear physics research, the reaction allows the study of the structure and properties of atomic nuclei, as well as nuclear reaction mechanisms. The photoneutron reaction to produce ^{64}Cu has advantages over traditional methods, such as avoiding the use of rare and expensive ^{64}Ni targets and complex chemical separation. In addition, the ^{64}Cu(n, γ)^{65}Cu reaction plays a key role in the quality control of the medical isotope ^{64}Cu. It helps assess the potential loss of ^{64}Cu during neutron irradiation and provides valuable data for understanding the nucleosynthesis of elements of medium mass in stars through neutron capture processes.

In the last century, laboratories worldwide have conducted experimental studies on the photoneutron reaction of ^{65}Cu using bremsstrahlung (BR) sources [11, 12] and positron annihilation in flight (PAIF) sources [13] using the activation method. Varlamov et al. [14] evaluated the existing ^{65}Cu(γ,n) experimental data, which showed considerable differences. The evaluated and experimental cross sections show that BR and PAIF are close within the low incident γ energy range but differ significantly in the high γ energy range, reflecting systematic errors in the experiment caused by the misclassification of neutron channels [8]. The quasi-monochromatic γ-ray source generated by laser Compton scattering provides an opportunity to measure the (γ, n) reaction, which helps distinguish the differences in the existing data.

In this study, the cross sections of the $^{\mathrm{nat}}$Cu(γ, n) reaction were measured within the giant dipole resonance (GDR) energy region using the SLEGS beamline [15] at the SSRF [16–18]. The ^{65}Cu(γ, n) cross sections were determined via the substitute method via the previously measured ^{63}Cu(γ, n) reaction. Furthermore, neutron capture cross sections for ^{64}Cu were also extracted. The remainder of this paper is organized as follows. Section 2 describes the experimental procedure for the $^{\mathrm{nat}}$Cu(γ, n) cross sections. Section 3 presents the methods for processing the experimental data of the photoneutron cross section and the results of the quasi-monochromatic and monochromatic cross sections of ^{65}Cu(γ, n) obtained by the subtraction method. Section 4 discusses the discrepancies between the measured data and existing experimental data, as well as the extraction of the radiative neutron capture cross section of ^{64}Cu. Finally, a brief conclusion is given in Sect. 5.

2 Experiment

This experiment was performed at the SLEGS beamline station [19] in the SSRF. The beamline uses inverse Compton scattering technology: 3.5 GeV electrons in the SSRF storage ring collide with photons from a 10.64 µm-wavelength, 100 W CO_2 laser, generating quasi-monochromatic gamma rays with tunable energies from 0.66 to 21.7 MeV. The energy of the γ beam was adjusted in slant-scattering mode with a minimum step of 10 keV. For measurements of the (γ, n) reactions at SLEGS, see Refs. [20–23] for details. A

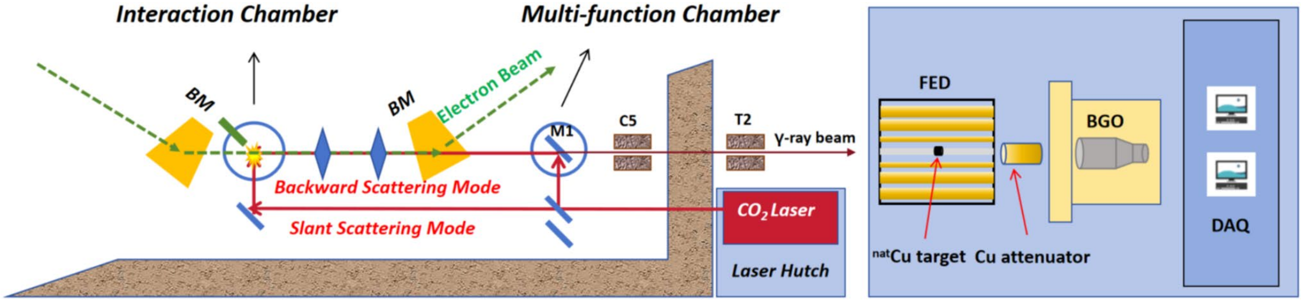

Fig. 1 (Color online) Schematic layout of the SLEGS beamline

schematic illustration of SLEGS and the corresponding experimental setup are presented in Fig. 1.

The cross sections for the ^{nat}Cu(γ, n) reaction were measured at 44 energy points ranging from 10.9 MeV ($\theta = 90°$) to 17.8 MeV ($\theta = 130°$). For each angle, the measurement time and neutron statistics were as follows: 2 h with neutron statistics exceeding 1.0×10^4 for $\theta \le 98°$, 1 h with neutron statistics exceeding 4.3×10^4 for $99° \le \theta \le 105°$, and 0.5 h with neutron statistics exceeding 4.8×10^4 for $\theta \ge 106°$. After passing through the collimation system, the laser Compton scattering (LCS) γ beam irradiated the experimental target positioned at the center of the ^{3}He flat-efficiency detector (FED) array [24]. The in-beam gamma flux was monitored using a large-volume BGO detector downstream of the FED. The incident γ spectrum was reconstructed using the direct unfolding method combined with a Geant4-simulated detector-response matrix (Fig. 2, see Refs. [25–27] for details).

2.1 Targets

The ^{nat}Cu target (3.15 g) was placed in polyethylene target holders and irradiated by LCS γ beams. The alignments of the target and FED with the LCS γ-ray beam were adjusted using a MiniPIX X-ray pixel detector for collimation. The detailed specifications are provided in Table 1.

The target holder has a 10 mm in diameter window. Considering that the size of the LCS γ-ray beams was approximately 4 mm in diameter at the target position, a 10 mm diameter window was sufficient for the target to be measured, avoiding the influence of neutrons from polythene.

Table 1 The information of ^{nat}Cu targets used in experiments

Target	Weight (g)	Diameter (mm)	Total thickness (mm)	Measured density (g/cm^3)
^{nat}Cu	3.15	10.00	4.48	8.69

Total chemical purity: ^{nat}Cu > 99.99%

2.2 Measurements

The SLEGS facility features a new FED with 26 proportional counters arranged in three concentric radii within a polyethylene moderator shielded by a 2 mm Cd sheet [23]. The counters, with an effective length of 500 mm and filled with ^{3}He gas at a pressure of 2 atm, were read out through the Mesytec MDPP-16 digitizers and MVME DAQ. Figure 3 shows the efficiency curves of each ring and the total efficiency curve simulated by GEANT4 using a real detector configuration. For the neutron evaporation spectrum, the total detector efficiency increases from 35.64% at 50 keV to 42.32% at 1.65 MeV, and then decreases slowly to 39.05% at 4 MeV [28]. The efficiency calibrated using the ^{252}Cf source is 42.10 ± 1.25%, corresponding to an average neutron energy of 2.13 MeV. In our experiment, we used the ring-ratio technique to obtain the average energy of neutrons produced by the (γ, n) reaction and then estimated the detector efficiency using its calibration curve [29, 30].

Fig. 2 (Color online) The energy spectrum of incident γ ray beams in the experiments

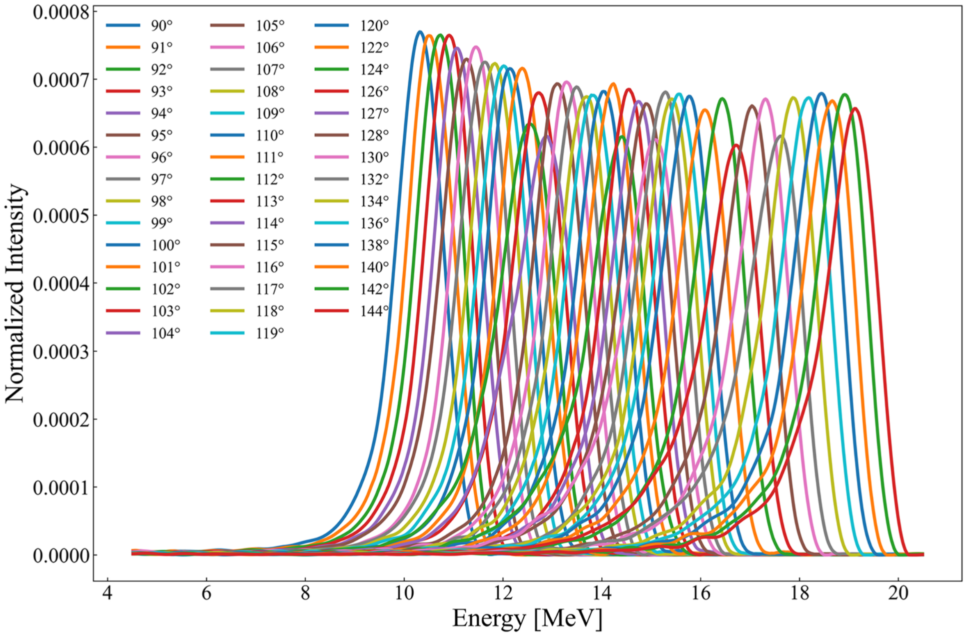

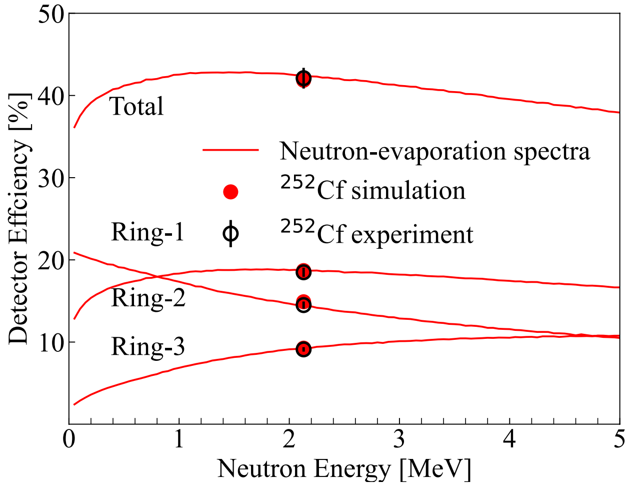

Fig. 3 (Color online) Total detector efficiency and efficiencies of individual rings. Detector efficiency curves were simulated using neutron evaporation spectra and monochromatic neutrons. The red dots are given by the neutron spectrum described by the Maxwell–Boltzmann distribution, at the average neutron energy (T = 1.42 MeV) of ^{252}Cf [28]

3 Data analysis and substitution measurement method

3.1 Data analysis method

In the monochromatic approximation, the photoneutron cross section can be expressed by the integral equation [31]:

$$\int_{S_\mathrm{n}}^{E_\mathrm{max}} n_\gamma(E)\sigma(E)\mathrm{d}E = \frac{N_\mathrm{n}}{N_\gamma N_\mathrm{t}\xi\epsilon_\mathrm{n}}, \tag{1}$$

where $n_\gamma(E)$ is the energy distribution of the LCS γ-ray beam normalized in the integration region. $\sigma(E)$ represents the photoneutron cross section, N_n the number of detected neutrons, N_t the number of target nuclei per unit area, and N_γ the number of incident γ-ray with energies above the neutron threshold. The self-attenuation coefficient ξ is given by [32]

$$\xi = \frac{\mu t}{1 - e^{-\mu t}}, \tag{2}$$

where μ is the linear attenuation coefficient of the sample and t is the thickness of the sample. The photoneutron cross section in the monochromatic approximation is calculated by

$$\sigma_{(\gamma,\mathrm{n})}^{E_\mathrm{max}} = \frac{N_\mathrm{n}}{N_\gamma N_\mathrm{t}\xi\epsilon_\mathrm{n}}. \tag{3}$$

In the experiment, the laser pulse cycle was 1000 μs (50 μs on + 950 μs off). Owing to the energy dispersion of LCS γ-ray beams, the monochromatic approximation is insufficient for determining photoneutron cross sections. When neutrons were counted with the FED array, the flat-efficiency regions for each detector ring were determined, considering the neutron energy and detector parameters. The median method was used to establish the optimal efficiency points and improve neutron count statistics.

To solve this unfolding problem, the integral in Eq. (1) is approximated as the summation of each γ beam profile, resulting in a system of linear equations $\sigma_\mathrm{f} = \mathbf{D}\sigma$ [33, 34]. The folding iteration method was used to solve this underdetermined system. Starting with a constant trial function σ_0, the folded vector $\sigma_\mathrm{f}^0 = \mathbf{D}\sigma^0$ was calculated [35–38]. The next trial input function σ_1 was obtained by adding the difference between the experimental spectrum σ_exp and the folded spectrum σ_f^0 to $\mathbf{D}\sigma^0$ after spline interpolation to match the vector dimensions. The iteration proceeds with [39–41]

$$\sigma^{i+1} = \sigma^i + (\sigma_\mathrm{exp} - \sigma_\mathrm{f}^i). \tag{4}$$

The iteration continues until convergence, when σ_f^{i+1} approximates σ_exp within statistical errors. Convergence was assessed by calculating the reduced χ^2 between σ_f^{i+1} and σ_exp, with typical convergence achieved in approximately three iterations, resulting in a reduced χ^2 value of approximately 1.

3.2 Substitution measurement method

In this experiment, the natural Cu target ($^\mathrm{nat}$Cu) has an isotopic abundance of 69.15% for ^{63}Cu and 30.85% for ^{65}Cu. The one-neutron (S_n) and two-neutrons (S_2n) separation energies for ^{63}Cu are 10.86 and 19.74 MeV, respectively. And for ^{65}Cu, S_n and S_2n become 9.91 MeV and 17.83 MeV, respectively [42–44]. Within the energy range where the one-neutron separation energy thresholds of ^{63}Cu and ^{65}Cu overlap, the FED detector measures neutrons from both the ^{63}Cu(γ, n) and ^{65}Cu(γ, n) reactions as

$$N_{^\mathrm{nat}\mathrm{Cu}} = N_{^{63}\mathrm{Cu}} + N_{^{65}\mathrm{Cu}}, \tag{5}$$

where $N_{^\mathrm{nat}\mathrm{Cu}}$ represents the result obtained from direct measurement, whereas $N_{^{63}\mathrm{Cu}}$ needs to be calculated by combining the monoenergy cross section $\sigma_{(\gamma,\mathrm{n})}^{^{63}\mathrm{Cu}}$ with the current energy spectrum $n_\gamma(E_\gamma)$; the detailed calculation process is shown in Eq. (6), where d is the thickness of target.

$$\begin{aligned} N_{^{63}\mathrm{Cu}} = N_\mathrm{t} g \epsilon_\mathrm{n} & \frac{\int_{S_\mathrm{n}}^{E_\mathrm{max}} n_\gamma \mathrm{d}E_\gamma \left(1 - e^{-\mu_{^\mathrm{nat}\mathrm{Cu}}\rho_{^\mathrm{nat}\mathrm{Cu}} d}\right)}{\mu_{^\mathrm{nat}\mathrm{Cu}}\rho_{^\mathrm{nat}\mathrm{Cu}} d} \\ & \times \int_{S_\mathrm{n}}^{E_\mathrm{max}} n_\gamma(E_\gamma)\sigma_{(\gamma,\mathrm{n})}^{^{63}\mathrm{Cu}}(E_\gamma)\mathrm{d}E_\gamma. \end{aligned} \tag{6}$$

By substituting the neutron count of $N_{^{63}\mathrm{Cu}}$ into Eq. (7), the quasi-monoenergetic photoneutron cross section data of ^{65}Cu can be obtained as

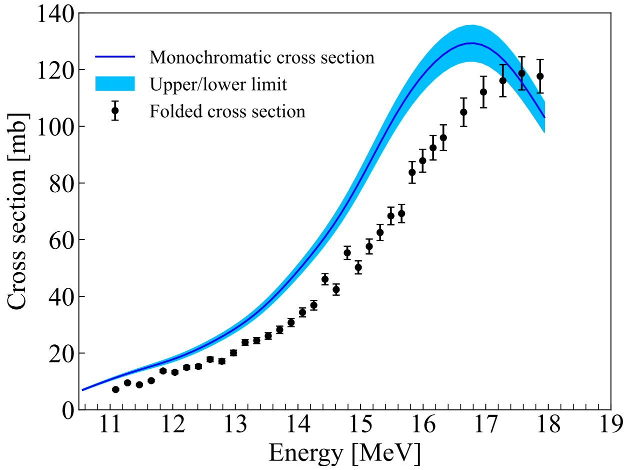

Fig. 4 (Color online) Cross sections of ^{65}Cu(γ, n) measured at SLEGS. The dots are the folded cross section, and the line with shaded area is the unfolded (monochromatic) cross section

$$\sigma^{^{65}\mathrm{Cu}}_{(\gamma,\mathrm{n})} = \int_{S_\mathrm{n}}^{E_\mathrm{max}} n_\gamma(E)\sigma(E)\mathrm{d}E = \frac{N_{^{\mathrm{nat}}\mathrm{Cu}} - N_{^{63}\mathrm{Cu}}}{N_\gamma N_\mathrm{t}\xi\epsilon_\mathrm{n}}. \tag{7}$$

The monochromatic cross section of the ^{65}Cu(γ, n)^{64}Cu reaction was derived using a deconvolution iteration method. Figure 4 compares the quasi-monoenergetic and monochromatic cross sections of ^{65}Cu.

According to Eq. (7), statistical uncertainty is mainly caused by N_n. Methodological uncertainty arises from the extraction algorithm N_n and deconvolution method incorporating the simulated BGO response matrix. Systematic uncertainty, which is the main source of the total error, includes the γ-flux uncertainty from the copper attenuator, the uncertainty of the target thickness, and the uncertainty of the FED efficiency. Table 2 summarizes the systematic and methodological uncertainties.

Table 2 Summary of (γ,n) cross-sectional uncertainties for measurements at SLEGS

Error source	Type	Uncertainty
FED efficiency	Systematic	3.02%
External copper	Systematic	0.50%
Target thickness	Systematic	<0.10%
N_n extraction algorithm	Data processing	2.00%
Unfolding method	Data processing	1.00%

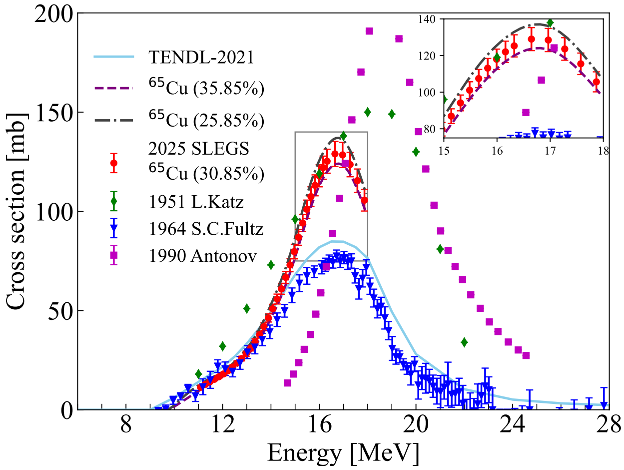

Fig. 5 (Color online) Cross section of ^{65}Cu(γ, n)^{64}Cu reaction. The solid circles denote the measured results with the natural abundance (30.85%) of ^{65}Cu. The results measured using BR γ rays by Katz [11] and Antonov [12] are plotted as solid green diamonds and purple squares, respectively. The results measured using PAIF γ rays by Fultz [13] are plotted as solid blue triangles. The TENDL-2021 evaluation is indicated by a sky-blue solid line. The calculated results by the increased (+5.00%) and decreased (−5.00%) abundance of ^{65}Cu are indicated by the purple line segment and gray dotted line. The inset figure highlights the differences in cross sections at the peak positions for these isotopic abundances

4 Results and discussion

4.1 ^{65}Cu photoneutron reaction cross section

The ^{65}Cu(γ, n)^{64}Cu photoneutron cross-sectional data measured at SLEGS were compared with the existing experimental and evaluated data in Fig. 5. Although the overall trends were consistent, significant discrepancies were observed in the absolute values. The experiment by Fultz et al. [13] at Lawrence Livermore National Laboratory (LLNL) is closest to the results in this work. They used BF$_3$ neutron detectors and measured in the energy range of 9.34 to 27.78 MeV. Data from Katz et al. [11] using BR source at the BETAT accelerator in Canada with a 22 MeV endpoint energy are notably higher than the LLNL data. Antonov's [12] measurements using the BR source at JINR are significantly higher than those of other datasets in terms of both neutron threshold and cross-sectional values. The cross section for ^{65}Cu(γ, n)^{64}Cu reaction measured by the monoenergetic LCS-γ source at SLEGS is listed in Table 3. Data errors include statistical, methodological, and systematic uncertainties. The total uncertainties at different E_γ are also listed in Table 3.

Isotopic abundance variations influence cross sections and cause discrepancies in the results. The photoneutron cross sections changed regularly with alterations in ^{65}Cu abundance. Based on data from the 2025 SLEGS experiment, comparing the cross section of ^{65}Cu at 35.85%, natural

Table 3 The monochromatic cross sections of ^{65}Cu(γ, n)^{64}Cu measured at SLEGS by substitution method

E_γ (MeV)	Cross sections (mb)	Statistical uncertainty (mb)	Systematical uncertainty (mb)	Methodological uncertainty (mb)	Total uncertainty (mb)
11.09	11.38	0.26	0.08	0.16	0.42
11.28	12.80	0.22	0.12	0.21	0.49
11.47	14.13	0.21	0.13	0.23	0.58
11.66	15.39	0.19	0.17	0.30	0.67
11.85	16.67	0.19	0.23	0.40	0.76
12.03	18.07	0.19	0.26	0.45	0.85
12.22	19.69	0.20	0.30	0.51	0.94
12.41	21.54	0.19	0.33	0.59	1.03
12.60	23.61	0.28	0.38	0.66	1.12
12.78	25.84	0.31	0.40	0.71	1.20
12.97	28.29	0.31	0.46	0.79	1.29
13.16	31.04	0.33	0.50	0.82	1.41
13.34	34.21	0.32	0.54	0.89	1.54
13.53	37.85	0.33	0.57	0.95	1.70
13.71	41.91	0.29	0.65	1.06	1.88
13.89	46.31	0.42	0.71	1.18	2.07
14.07	50.93	0.43	0.78	1.30	2.27
14.25	55.79	0.54	0.85	1.37	2.48
14.43	60.93	0.56	0.98	1.61	2.70
14.61	66.59	0.45	1.01	1.62	2.95
14.79	72.81	0.52	1.19	1.94	3.25
14.96	79.64	0.47	1.16	1.93	3.58
15.14	86.86	0.51	1.34	2.21	3.95
15.31	94.16	0.50	1.45	2.43	4.34
15.48	101.13	0.53	1.59	2.64	4.71
15.66	107.55	0.51	1.65	2.75	5.07
15.82	113.23	0.63	1.93	3.20	5.40
15.99	118.06	0.66	2.06	3.40	5.70
16.16	122.15	0.68	2.20	3.62	5.97
16.32	125.43	0.70	2.33	3.84	6.20
16.65	129.18	0.60	2.57	4.26	6.51
16.96	128.71	0.60	2.78	4.77	6.58
17.27	123.81	0.68	2.84	4.85	6.39
17.58	115.61	0.82	2.97	4.97	6.01
17.87	105.68	0.81	2.98	5.03	5.52

abundance (30.85%), and 25.85%, the photoneutron cross sections decreased as the abundance of ^{65}Cu increased (e.g., from 25.85% to 35.85%) and increased as the abundance decreased (see the inset in Fig. 5). This occurs across all energy ranges and is most noticeable near the threshold and peak positions in the cross-sectional distribution. It is suggested that the isotopic abundances in the target material should be determined prior to analysis of the substitution data. The sensitive change in isotopic abundance also suggests that it is capable of adopting an enhanced isotopic target to determine the cross section (γ, n) in addition to the pure isotopic target.

As discussed in Ref. [45], the ratios of the integral cross sections provide a clear indication of the systematic differences among the various data compilations. The integral cross sections in S_n and S_max regions are as follows:

$$\sigma^\mathrm{int} = \int_{S_\mathrm{n}}^{S_\mathrm{max}} \sigma(E)\mathrm{d}E. \tag{8}$$

Based on these experimental data, the integral ratios of the photoneutron reaction cross section were calculated for energy ranges from S_n to 15 MeV, 15 MeV to S_2n, and S_n to S_2n, and the results are presented in Table 4. In the energy

Table 4 Integral cross-sectional ratio

Ratio relation	σ^{int} ratio		
	S_n ~15 MeV	15 MeV ~ S_{2n}	S_n ~ S_{2n}
$\sigma^{\text{int}}_{\text{TENDL}}/\sigma^{\text{int}}_{\text{SLEGS}}$	1.04	0.68	0.80
$\sigma^{\text{int}}_{\text{Fultz}}/\sigma^{\text{int}}_{\text{SLEGS}}$	0.92	0.61	0.69
$\sigma^{\text{int}}_{\text{Katz}}/\sigma^{\text{int}}_{\text{SLEGS}}$	1.49	1.04	1.21
$\sigma^{\text{int}}_{\text{Antonov}}/\sigma^{\text{int}}_{\text{SLEGS}}$	0.23	0.77	0.68

range of S_n to 15 MeV, the measured results show a difference of only 0.8% from the Fultz data and a discrepancy of less than 0.4% from theoretical calculations of TENDL-2021, while discrepancies with other datasets exceed 40%. In the 15 MeV to S_{2n} range, the minimum difference between this study and the Katz [11] data is 0.4%, and the differences with other datasets exceed 20%. In general, the neutron threshold and the peak position of the cross section demonstrate good consistency with the results measured by Fultz [13] and the evaluation in TENDL-2021 [46]. The neutron threshold exhibits favorable agreement with Katz data [11]. However, there are notable differences in both the neutron threshold and peak position compared with the data measured by Antonov [12].

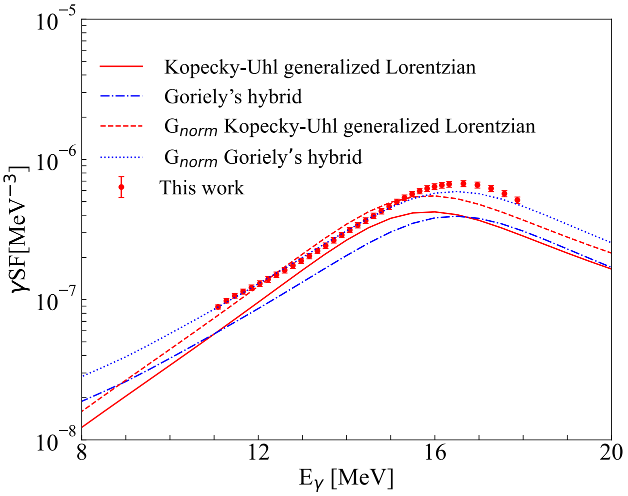

Fig. 6 (Color online) The γSF values of ^{65}Cu calculated using the Kopecky-Uhl generalized Lorentzian model (red solid line) and Goriely's hybrid model (blue dash-dot line) with default parameters are compared with those obtained from the optimized Kopecky-Uhl generalized Lorentzian model (red dashed line) and Goriely's hybrid model (blue dotted line) using the G_{norm} method, along with the γSF values extracted from the SLEGS experimental data (red plot points)

4.2 ^{64}Cu radiative neutron capture cross section

The gamma strength function (γSF) [47] is used to describe the average probabilities of gamma decay and absorption in nuclear reactions, and is an important parameter for characterizing the nuclear reaction process. When research involves reactions with gamma rays, such as reactions (n, γ) and (γ, n), the precision of γSF is particularly crucial. According to the principle of detailed balance [48] and generalized Brink assumption [49–51], it is believed that the upward $\overrightarrow{f_{X\ell}}(E_\gamma)$ is approximately equal to the downward $\overleftarrow{f_{X\ell}}(E_\gamma)$. Therefore, it can be considered that $f_{X\ell}(E_\gamma) \approx \overrightarrow{f_{X\ell}}(E_\gamma) \approx \overleftarrow{f_{X\ell}}(E_\gamma)$. The (upward) $\sigma_{\gamma n}$ photoneutron cross section is connected to the (downward) γSF [52] by

$$f_{X1}(E_\gamma) = \frac{1}{3\pi^2\hbar^2c^2}\frac{\sigma_{\gamma n}(E_\gamma)}{E_\gamma}, \tag{9}$$

in which the constant is $1/3\pi^2\hbar^2c^2 = 8.674\times10^{-8}$ mb^{-1} MeV^{-2}. Using this relationship, γSF can be obtained from the cross section measured in the photoneutron reaction. Then, the γSF model in TALYS was compared with the experimentally constrained γSF. The model prediction closest to the experimentally obtained γSF is selected. Furthermore, the γSF model is constrained using the normalization parameter G_{norm} in the TALYS 2.0 toolkit, and the optimization of the normalization parameter G_{norm} is achieved by minimizing the χ^2 value, thus making the theoretical calculation results of the constrained γSF model more consistent with the experimentally obtained γSF values. The γSF of ^{65}Cu(γ, n) constrained by measured (γ, n) data is shown in Fig. 6, with χ^2 determined by

$$\chi^2 = \frac{1}{N}\sum_{i=1}^{N}\left(\frac{\sigma_{\text{th},i}-\sigma_{\text{exp},i}}{\sigma_{\text{err},i}}\right)^2, \tag{10}$$

where N denotes the total number of experimental data points. $\sigma_{\text{th},i}$, $\sigma_{\text{exp},i}$ and $\sigma_{\text{err},i}$ denote the theoretical value, experimentally measured value, and experimental error of γSF at the i-th data point, respectively. The neutron capture cross section of ^{64}Cu, after adjustment of the optimal G_{norm} value, is shown in Fig. 7. Specifically, G_{norm} is set to 1.2 in the Kopecky-Uhl generalized Lorentzian model [53]. However, it is 1.4 in the Goriely hybrid model. In particular, when constrained by G_{norm}, the χ^2 value of the hybrid mode [54] was the smallest among all the investigated models, showing the best agreement with this set of experimental data. Similarly, Utsunomiya et al. [39] and Li et al. [44] previously conducted related research and measured the (n, γ) radiative reaction cross sections for the ^{136,137}Ba and ^{62}Cu isotopes. In this study, owing to the lack of experimental data on the low-lying excited states and neutron resonance spacings of ^{65}Cu, the constraints on the nuclear-level density (NLD) model are limited, resulting in substantial theoretical uncertainties. The study of the ^{64}Cu(n, γ) cross section is of great value for improving nuclear data and optimizing the

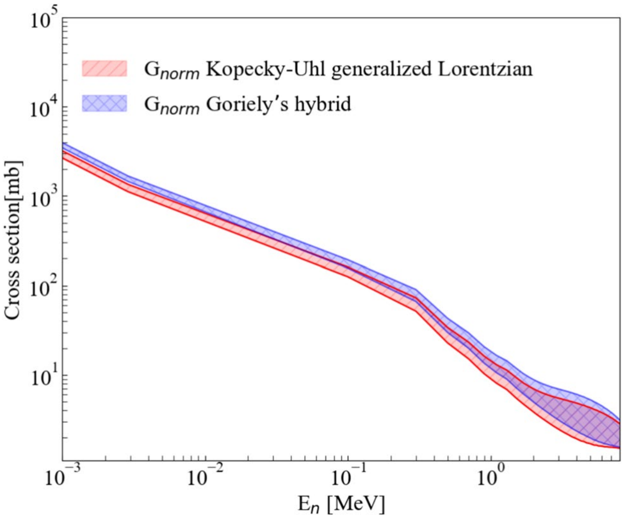

Fig. 7 (Color online) The cross sections for ^{64}Cu(n, γ)^{65}Cu are calculated using the optimized Kopecky-Uhl generalized Lorentzian model (red shaded area) and Goriely's hybrid model (purple shaded area). The shaded area represents the results considering six different nuclear-level density models within the TALYS 2.0 [51]

preparation of medical isotopes. This is closely related to the measurement of the ^{65}Cu(γ, n)^{64}Cu cross section through the principle of detailed balance, and the former can verify the reliability of the latter, collectively highlighting the overall significance of the research.

5 Summary

The reaction cross sections of $^{\mathrm{nat}}$Cu(γ, n) were measured in the incident energy range of 11.09 to 17.87 MeV using the ^{3}He FED detector array developed by SLEGS. Based on the measured photoneutron cross-sectional data and the previously measured results for ^{63}Cu(γ, n) at SLEGS, the reaction cross sections of ^{65}Cu(γ, n)^{64}Cu were obtained using the cross-sectional substitution method. Compared with existing experimental data, the reliability of this method was demonstrated, providing a new approach for photoneutron cross section measurements. Given the extensive application of ^{64}Cu in medical fields such as nuclear medicine imaging and tumor therapy, clarifying the existing discrepancies in the reaction cross sections of the ^{65}Cu(γ, n)^{64}Cu reaction is likely to play an important role in these fields. The sensitivity of the isotopic abundance change in the natural copper target shows that the enhanced purity of the specific isotope could be used to measure its (γ, n) cross section via the substitution measured in this work. The experimentally constrained γSF of ^{65}Cu was extracted from the ^{65}Cu(γ, n)^{64}Cu cross-sectional distribution. In addition, the cross-sectional curve of its inverse reaction, ^{64}Cu(n, γ), was calculated, which provides a new approach to the extraction of cross sections (n, γ) from some unstable nuclides.

Acknowledgements The authors thank the SSRF accelerator team for their stable maintenance of the electron beam during the experiments and the SLEGS (https://cstr.cn/31124.02.SSRF.BL03SSID) team for assistance in measurement and data analysis.

Author Contributions All authors contributed to the study conception and design. Material preparation, data collection, and analysis were performed by Zi-Rui Hao, Zhi-Cai Li, Qian-Kun Sun, Long-Xiang Liu, Hang-Hua Xu, Yue Zhang, Meng-Die Zhou, Wen Luo, Yu-Xuan Yang, Sheng Jin, Kai-Jie Chen, Shan Ye, Zhen-Wei Wang, Yu-Ting Wang, Hui-Ling Wei, Yao Fu, Kun Yu, Hong-Wei Wang, Gong-Tao Fan, and Chun-Wang Ma. The first draft of the manuscript was written by Pu Jiao, and all authors commented on previous versions of the manuscript. All authors read and approved the final manuscript.

Data Availability The data that support the findings of this study are openly available in Science Data Bank at https://cstr.cn/31253.11.sciencedb.j00186.00747 and https://doi.org/10.57760/sciencedb.j00186.00747.

Declarations

Conflict of interest Chun-Wang Ma and Hong-Wei Wang are editorial board members for Nuclear Science and Techniques and were not involved in the editorial review, or the decision to publish this article. All authors declare that there are no Conflict of interest.

References

1. W. Luo, Production of medical radioisotope ^{64}Cu by photoneutron reaction using ELI-NP γ-ray beam. Nucl. Sci. Tech. **27**, 96 (2016). https://doi.org/10.1007/s41365-016-0094-6
2. W. Luo, D.L. Balabanski, D. Filipescu, A data-based photonuclear simulation algorithm for determining specific activity of medical radioisotopes. Nucl. Sci. Tech. **27**, 113 (2016). https://doi.org/10.1007/s41365-016-0111-9
3. I.M. Jackson, P.J.H. Scott, S. Thompson, Clinical applications of radiolabeled peptides for PET. Semin. Nucl. Med. **47**, 493 (2017). https://doi.org/10.1053/j.semnuclmed.2017.05.007
4. M. Brandt, J. Cardinale, M.L. Aulsebrook et al., An overview of PET radiochemistry, part 2: radiometals. J. Nucl. Med. **59**, 1500 (2018). https://doi.org/10.2967/jnumed.117.190801
5. O.O. Krasnovskaya, D. Abramchuck, A. Erofeev et al., Recent advances in ^{64}Cu/^{67}Cu-based radiopharmaceuticals. Int. J. Mol. Sci. **24**, 9154 (2023). https://doi.org/10.3390/ijms24119154
6. M. Bobeica, D. Niculae, D. Balabanski et al., Radioisotope production for medical applications at ELI-NP. Rom. Rep. Phys. **68**, 847 (2016)
7. A. Boschi, P. Martini, E. Janevik-Ivanovska et al., The emerging role of copper-64 radiopharmaceuticals as cancer theranostics. Drug Discov. Today **23**, 1489 (2018). https://doi.org/10.1016/j.drudis.2018.04.002
8. F. Cantiello, V. Gangemi, G.L. Cascini et al., Diagnostic accuracy of ^{64}copper prostate-specific membrane antigen positron emission tomography/computed tomography for primary lymph node staging of intermediate-to high-risk prostate cancer: our preliminary

experience. Urology **106**, 139 (2017). https://doi.org/10.1016/j.urology.2017.04.019

9. B. Grubmüller, R.P. Baum, E. Capasso et al., ^{64}Cu-PSMA-617 PET/CT imaging of prostate adenocarcinoma: first in-human studies. Cancer Biother. Radiopharm. **31**, 277 (2016). https://doi.org/10.1089/cbr.2015.1964
10. G.A. Follacchio, M.S. De Feo, G. De Vincentis et al., Radiopharmaceuticals labelled with copper radionuclides: clinical results in human beings. Curr. Radiopharm. **11**, 22 (2018). https://doi.org/10.2174/1874471011666171211161851
11. H.E. Johns, L. Katz, R.E.A. Douglas et al., Gamma-neutron cross sections. Phys. Rev. **80**, 1062 (1950). https://doi.org/10.1103/PhysRev.80.1062
12. A.D. Antonov, N.P. Balabanov, Y.P. Gangrskii et al., Studies of photonuclear reactions with emission of α particles in the region of the giant dipole resonance. Sov. J. Nucl. Phys. **51**, 193 (1990)
13. S.C. Fultz, R.L. Bramblett, J.T. Caldwell et al., Photoneutron cross sections for natural Cu, Cu^{63}, and Cu^{65}. Phys. Rev. **133**, B1149 (1964). https://doi.org/10.1103/PhysRev.133.B1149
14. A.V. Varlamov, V.V. Varlamov, D.S. Rudenko *et al.*, Atlas of giant dipole resonances. Parameters and graphs of photonuclear reaction cross sections. INDC (NDS)-394, IAEA NDS, Vienna, Austria. **1–311** (1999). https://inis.iaea.org/records/4exm3-2ag10
15. L.X. Liu, H.W. Wang, G.T. Fan et al., The SLEGS beamline of SSRF. Nucl. Sci. Tech. **35**, 111 (2024). https://doi.org/10.1007/s41365-024-01469-3
16. R.Z. Tai, Z.T. Zhao, Overview of SSRF phase-II beamlines. Nucl. Sci. Tech. **35**, 137 (2024). https://doi.org/10.1007/s41365-024-01487-1
17. R.Z. Tai, Z.T. Zhao, Commissioning and first results of the SSRF phase-II beamline project. J. Phys. Conf. Ser. **2380**, 012004 (2022). https://doi.org/10.1088/1742-6596/2380/1/012004
18. H.W. Wang, G.T. Fan, L.X. Liu et al., Commissioning of laser electron gamma beamline SLEGS at SSRF. Nucl. Sci. Tech. **33**, 87 (2022). https://doi.org/10.1007/s41365-022-01076-0
19. K.J. Chen, L.X. Liu, Z.R. Hao et al., Simulation and test of the SLEGS TOF spectrometer at SSRF. Nucl. Sci. Tech. **34**(3), 47 (2023). https://doi.org/10.1007/s41365-023-01194-3
20. H.H. Xu, G.T. Fan, H.W. Wang et al., Interaction chamber for laser Compton slant-scattering in SLEGS beamline at Shanghai Light Source. Nucl. Instrum. Methods phys. Res. A **1033**, 166742 (2022). https://doi.org/10.1016/j.nima.2022.166742
21. Z.R. Hao, H.H. Xu, G.T. Fan et al., Gamma spot monitor at SLEGS beamline. Nucl. Instrum. Methods Phys. Res. A **1068**, 169748 (2024). https://doi.org/10.1016/j.nima.2024.169748
22. Z.C. Li, Y.X. Yang, Z.W. Cao et al., Effective extraction of photoneutron cross-section distribution using gamma activation and reaction yield ratio method. Nucl. Sci. Tech. **34**, 170 (2023). https://doi.org/10.1007/s41365-023-01330-z
23. M.D. Zhou, G.T. Fan, C.W. Ma et al., Measurement of ^{59}Co(γ, n)^{58}Co using a new flat-efffciency neutron detector at SLEGS. Phys. Rev. C **111**, 054612 (2025). https://doi.org/10.1103/PhysRevC.111.054612
24. Z.R. Hao, L.X. Liu, Y. Zhang et al., The day-one experiment at slegs: systematic measurement of the (γ, 1n) cross sections on ^{197}Au and ^{159}Tb for resolving existing data discrepancies. Science Bulletin. **70**, 2591–2597 (2025). https://doi.org/10.1016/j.scib.2025.05.037
25. L.X. Liu, H. Utsunomiya, G.T. Fan et al., Energy profile of laser compton slant-scattering γ-ray beams determined by direct unfolding of total-energy responses of a BGO detector. Nucl. Instrum. Methods Phys. Res. A **1063**, 169314 (2024). https://doi.org/10.1016/j.nima.2024.169314
26. W. Luo, H.Y. Lan, Y. Xu et al., Implementation of the n-body Monte-Carlo event generator into the Geant4 toolkit for photonuclear studies. Nucl. Instrum. Methods Phys. Res. A **849**, 49 (2017). https://doi.org/10.1016/j.nima.2017.01.010
27. S. Agostinelli, J. Allison, K.A. Amako et al., Geant4-a simulation toolkit. Nucl. Instrum. Methods Phys. Res. A **506**, 250 (2003). https://doi.org/10.1016/S0168-9002(03)01368-8
28. Z.R. Hao, G.T. Fan, L.X. Liu et al., Design and simulation of 4π flat-efficiency ^{3}He neutron detector array. Nucl. Tech. (in Chinese) **43**, 9 (2020). https://doi.org/10.11889/j.0253-3219.2020.hjs.43.110501
29. B. Berman, J. Caldwell, R. Harvey et al., Photoneutron cross sections for ^{90}Zr, ^{91}Zr, ^{92}Zr, ^{94}Zr, and ^{89}Y. Phys. Rev. **162**, 1098 (1967). https://doi.org/10.1103/PhysRev.162.1098
30. O. Itoh, H. Utsunomiya, H. Akimune et al., Photoneutron cross sections for Au revisited: measurements with laser compton scattering γ-rays and data reduction by a least-squares method. J. Nucl. Sci. Technol. **48**, 834 (2011). https://doi.org/10.1080/18811248.2011.9711766
31. J.W. Jury, B.L. Berman, D.D. Faul et al., Photoneutron cross sections for ^{13}C. Phys. Rev. C **19**, 1684 (1979). https://doi.org/10.1103/PhysRevC.19.1684
32. National Institute of Standards and Technology (NIST), X-ray mass attenuation coefficients. (2025). https://www.physics.nist.gov/PhysRefData/XrayMassCoef/chap2.html
33. Y.L. Dang, L.F. Long, F.G. Yong *et al.*, New measurement of thick target yield for narrow resonance at $E_x = 9.17$ MeV in the ^{13}C$(p, \gamma)^{14}$N reaction. Chin. Phys. B **28**, 060706 (2019). https://doi.org/10.1088/1674-1056/ab96a0
34. F.L. Liu, W.S. Yang, J.H. Wei et al., Study on γ-ray source from the resonant reaction ^{19}F$(p, \alpha\gamma)^{16}$O at $e_p = 340$ keV. Chin. Phys. B **29**, 070702 (2020). https://doi.org/10.1088/1674-1056/ab96a0
35. M. Guttormsen, T.S. Tveter, L. Bergholt et al., The unfolding of continuum γ-ray spectra. Nucl. Instrum. Methods Phys. Res. A **374**, 3 (1996). https://doi.org/10.1016/0168-9002(96)00197-0
36. H. Utsunomiya, I. Gheorghe, D.M. Filipescu et al., Direct neutron-multiplicity sorting with a flat-efficiency detector. Nucl. Instrum. Methods Phys. Res. A **871**, 135 (2017). https://doi.org/10.1016/j.nima.2017.08.001
37. I. Gheorghe, H. Utsunomiya, S. Katayama et al., Photoneutron cross-section measurements in the ^{209}Bi(γ, xn) reaction with a new method of direct neutron-multiplicity sorting. Phys. Rev. C **96**, 044604 (2017). https://doi.org/10.1103/PhysRevC.96.044604
38. I. Gheorghe, H. Utsunomiya, K. Stopani et al., Updated neutron-multiplicity sorting method for producing photoneutron average energies and resolving multiple firing events. Nucl. Instrum. Methods Phys. Res. A **1019**, 165867 (2021). https://doi.org/10.1016/j.nima.2021.165867
39. T. Renstrøm, H. Utsunomiya, H.T. Nyhus et al., Verification of detailed balance for γ absorption and emission in Dy isotopes. Phys. Rev. C **98**, 054310 (2018). https://doi.org/10.1103/PhysRevC.98.054310
40. G.C. Yang, L.M. Hua, F. Lu et al., Response functions of a 4 π summing gamma detector in β-olso method. Nucl. Sci. Tech. **33**, 68 (2022). https://doi.org/10.1007/s41365-022-01058-2
41. P. Jiao, Z.R. Hao, Q.K. Sun et al., Measurements of ^{27}Al(γ, n) reaction using quasi-monoenergetic γ beams from 13.2 to 21.7 MeV at SLEGS. Nucl. Sci. Tech. **36**, 66 (2025). https://doi.org/10.1007/s41365-025-01662-y
42. W.J. Huang, M. Wang, F.G. Kondev et al., The AME 2020 atomic mass evaluation (I). Evaluation of input data, and adjustment procedures. Chin. Phys. C **45**, 030002 (2021) https://doi.org/10.1088/1674-1137/abddb0
43. M. Wang, W.J. Huang, F.G. Kondev et al., The AME 2020 atomic mass evaluation (II). Tables, graphs and references. Chin. Phys. C **45**, 030003, (2021). https://doi.org/10.1088/1674-1137/abddaf

44. Z.C. Li, Z.R. Hao, Q.K. Sun et al., New measurement of ^{63}Cu(γ, n)^{62}Cu cross-section using quasi-monoenergetic γ-ray beam. Nucl. Sci. Tech. **36**, 34 (2025). https://doi.org/10.1007/s41365-024-01631-x
45. V. Varlamov, B. Ishkhanov, V. Orlin, Reliability of (γ, 1n),(γ, 2n), and (γ, 3n) cross-section data on ^{159}Tb. Phys. Rev. C **95**, 054607 (2017). https://doi.org/10.1103/PhysRevC.95.054607
46. TENDL-2021, https://tendl.web.psi.ch/tendl_2021/gamma_html/gamma.html, (2021)
47. J. Kopecky, M. Uhl, Test of gamma-ray strength functions in nuclear reaction model calculations. Phys. Rev. C **41**, 1941 (1990). https://doi.org/10.1103/PhysRevC.41.1941
48. J.M. Blatt, V.F. Weisskopf, F.J. Dyson et al., Theoretical nuclear physics. Physics Today **6**, 17 (1953). https://doi.org/10.1063/1.3061164
49. H. Utsunomiya, T. Renstrϕm, G. M.Tveten et al., Photoneutron cross sections for Ni isotopes: Toward understanding (n,γ) cross sections relevant to weak s-process nucleosynthesis. Phys. Rev. C **98**, 054619 (2018). https://doi.org/10.1103/PhysRevC.98.054619
50. D. Filipescu, I. Gheorghe, H. Utsunomiya et al., Photoneutron cross sections for samarium isotopes: toward a unified understanding of (γ, n) and (n,γ) reactions in the rare earth region. Phys. Rev. C **90**, 064616 (2014). https://doi.org/10.1103/PhysRevC.90.064616
51. A. Koning, TEFAL-2.0, Making ENDF-6 nuclear data libraries with TALYS, https://nds.iaea.org/talys/tutorials/tefal.pdf (2023)
52. R. Capote, M. Herman, P. Obložinskỳ et al., Ripl-reference input parameter library for calculation of nuclear reactions and nuclear data evaluations. Nucl. Data Sheets **110**, 3107 (2009). https://doi.org/10.1016/j.nds.2009.10.004
53. S. Goriely, V. Plujko, Simple empirical E1 and M1 strength functions for practical applications. Phys. Rev. C **99**, 014303 (2019). https://doi.org/10.1103/PhysRevC.99.014303
54. E.B. Balbutsev, I.V. Molodtsova, P. Schuck, Spin scissors mode and the fine structure of M1 states in nuclei. Nucl. Phys. A **872**, 1 (2011). https://doi.org/10.1016/j.nuclphysa.2011.09.016